Heliyon

Received:
20 November 2017
Revised:
31 July 2018
Accepted:
3 September 2018

Cite as: Vincent Roth, Tatenda Lemann, Gete Zeleke, Alemtsehay Teklay Subhatu, Tibebu Kassawmar Nigussie, Hans Hurni. Effects of climate change on water resources in the upper Blue Nile Basin of Ethiopia. Heliyon 4 (2018) e00771. doi: 10.1016/j.heliyon.2018.e00771

Effects of climate change on water resources in the upper Blue Nile Basin of Ethiopia

Vincent Roth [a,b,*], **Tatenda Lemann** [a,b], **Gete Zeleke** [a,c], **Alemtsehay Teklay Subhatu** [a,b], **Tibebu Kassawmar Nigussie** [b,c], **Hans Hurni** [a]

[a] *Centre for Development and Environment (CDE), Mittelstrasse 43, 3012 Bern, Switzerland*

[b] *Integrative Geography – Sustainable Land Management Group, University of Bern, Switzerland*

[c] *Water and Land Resource Centre, Addis Abeba, Ethiopia*

* Corresponding author at: Centre for Development and Environment (CDE), Mittelstrasse 43, 3012 Bern, Switzerland.
E-mail address: vincent.roth@cde.unibe.ch (V. Roth).

Abstract

Drawing on hydrology, rainfall, and climatic data from the past 25 years, this article investigates the effects of climate change on water resources in the transnational Blue Nile Basin (BNB). The primary focus is on determining the long-term temporal and seasonal changes in the flows of the Blue Nile in Ethiopia at the border to Sudan. This is important because the Blue Nile is the main tributary to the Nile river, the lifeline of both Sudan and Egypt. Therefore, to begin with long-term trends in hydrological time series were detected by means of both parametric and nonparametric techniques. The Soil and Water Assessment Tool (SWAT) model was calibrated using several sub-basins and new high-resolution land use and soil maps. Future climate change impacts were projected using data from the Climate Forecast System Reanalysis (CFSR) of the National Centers for Environmental Predictions based on three different climate change scenarios from the Coupled Model Intercomparison Project (CMIP3). Projected time series were analysed for changes in rainfall and streamflow trends. Climate change scenario modelling suggested that the precipitation will increase from 7% to 48% and that streamflow from the BNB could increase by 21% to 97%. The results provide a basis for evaluating future impacts of climate change on the upper Blue Nile River (Abay River). This is the main river basin contributing to the Nile and a source of water for millions of people in Sudan and Egypt, downstream from Ethiopia. Three models

https://doi.org/10.1016/j.heliyon.2018.e00771

(CCCMA, CNRM, MRI) were applied in this research, within two future time periods (2046–2064 and 2081–2099) and one scenario (A1B). The Abay Basin was divided into seven sub-basins, six of which were used as inlets to the lowest basin at the border to Sudan. The above-mentioned results show that under current climate change scenarios there is a strong seasonal shift to be expected from the present main rainfall season (June to September) to an earlier onset from January to May with less pronounced peaks but longer duration of the rainfall season. This has direct consequences on the streamflow of the Blue Nile, which is connected to the rainfall season and therefore has direct effects on the people living in the sphere of influence of the Nile River.

Keywords: Environmental science, Geography, Geoscience, Hydrology

1. Introduction

The upper Blue Nile Basin (uBNB) in the Highlands of Ethiopia plays a key role in the hydrology of the Nile region. More than 60% of the total Nile river streamflow that reaches Sudan and Egypt is generated in the Ethiopian part of the BNB. This hydrological imbalance has, in the past, caused controversy and dissatisfaction among the affected riverine countries. With climate change looming and uncertainty rising as to its potential impacts, research is needed that examines how possible changes might affect the region. The potential impacts of climate change on the Nile Basin are of particular concern given their geopolitical and socio-economic implications (Niang et al., 2014). The Blue Nile is expected to have a lower streamflow by the end of the 21st century because of declining precipitation and increasing use of water for irrigation and hydropower (Elshamy et al., 2009; Mccartney et al., 2012). Accordingly, Beyene and Meissner (2010) estimated that Nile flows will first increase until mid-century, and then begin declining under scenarios A2 and B1 (see subsection 5.2 on page 17 for details) because of increased evaporation and declining rainfall. Abdo et al. (2009) projected a decline of outflow from Lake Tana by 2080, while Taye et al. (2011) reported inconclusive findings as to possible changes in runoff. There have been several studies on future hydroclimatic variability impacting the BNB (Adem et al., 2016; Aich et al., 2014; Arsano and Tamrat, 2005; Beyene and Meissner, 2010; Sutcliffe and Parks, 1999) as well as on corresponding historic variability (Conway, 2000; Kebede et al., 2006; Mccartney et al., 2012). Very few studies have coupled climate change models with watershed models (Adem et al., 2016; Beyene et al., 2009; Wagena et al., 2016). Model coupling is critical to assess the possible impacts of climate change on both regional water resources and local landscape erosion. Most of the relevant studies used low-resolution spatial input data (FAO, SRTM, global land cover) and a limited number of gauges for calibration (Aich et al., 2014). Taye et al. (2015) compared several

 https://doi.org/10.1016/j.heliyon.2018.e00771

studies on climate change in the BNB. They reported changes in future streamflow from 10% to 94%. Beyene et al. (2009) reported projections of precipitation increase as high as 25% by the end of the century (2070–2099).

Future water resource development in the BNB will be driven predominantly by hydropower and agriculture needs, requiring large volumes of stored water (Mccartney et al., 2012). The Ethiopian government is currently implementing the Grand Ethiopian Renaissance Dam near the Ethiopia–Sudan border. It will have a major impact on the region. There is an increasing need for corresponding estimates of current and future streamflows. At the same time, strong scientific evidence indicates that average global temperature (IPCC (Intergovernmental Panel for Climate Change), 2008) will rise 1.4–5.8 °C by 2100, with average sea levels rising 10 cm over the same period. However, climate scenarios are expected to vary considerably in time and space, affecting climatic and meteorological variables very differently depending on the region, with major impacts on local natural environments and human systems. Whatever the case, any change in average global temperature will affect the spatial and temporal occurrence of rainfall. This, in turn, will affect hydrological cycles, water balances, and the resulting availability of water resources. Intergovernmental Panel on Climate Change (IPCC) findings indicate that a country like Ethiopia will most likely be more vulnerable to climatic change because of its particular climatic, hydrologic, and economic circumstances. Estimating future rainfall changes over sub-Saharan Africa remains challenging; nevertheless, in regions with high or complex topography like Ethiopia, downscaled projections point to increases in rainfall and extreme rainfall (Niang et al., 2014). Notably, Ethiopia mainly depends on rainfed agriculture and available water resources in the Highlands, while large parts of its southern and eastern regions are extremely arid and prone to drought and desertification.

The present study seeks to assess the impacts of climate change on the hydrological regime of the Abay Basin in the 21st century, using statistically robust globally modelled climate data that possess a climate change component. To date, research on basin characteristics, hydrology, and climatic conditions in the upper BNB has been meagre and relatively fragmented (Conway, 1997; Dessie et al., 2014; Mishra et al., 2004). Further, the reliability and availability of hydrological and meteorological data for the region are very limited, and the data that are available display poor quality and large gaps.

Kim and Kaluarachchi (2009) evaluated the impact of six climate change scenarios on water resources in Ethiopia's upper BNB, using weighted values of outcomes. They relied on two streamflow stations (El Deim and Kessie) for the entire BNB as well as nine weather stations (from the National Meteorology Agency) for climate data. Their results did not include goodness of fit for the model used and only reflected changes in flow regimes for different scenarios. Their results

 https://doi.org/10.1016/j.heliyon.2018.e00771

indicated increasing rainfall in the dry season coupled with increasing flood risks in downstream countries based on high-flow statistics. In a separate study focused on the implications of climate change for hydrological extremes in the BNB, Taye et al. (2011) concluded that the overall trend emerging from many different streamflow projections is towards increasing high and low flows, leading to a reduction in drought events.

Legesse Gebre and Fulco (2015) used the Hydrologic Engineering Center-Hydrological Modelling System (HEC-HMS 3.5) model to simulate the effects of two climate change scenarios on the hydrological regimes of the upper Blue Nile catchment. They concluded that Nile river flows would increase from 74.8% to 127.4% for these two scenarios.

Nawaz et al. (2010) used General Circulation Models (GCM) downscaling and the Nile Forecasting Centre (NFS) model for sensitivity analysis to climate change of the Blue Nile runoff with outputs from three GCMs forced with two IPCC Special Reports on Emission Scenarios (SRES) greenhouse gas emission scenarios. Their results indicate wetter conditions and increased average and extreme flows.

Adem et al. (2016) used A2 and B2 emission scenarios (see subsection 5.2 on page 17 for details) to analyse climate change effects on the upper Gilgel Abay using the Soil and Water Assessment Tool (SWAT) and the HadCM3 from the Hadley Centre in the UK. They concluded that both scenarios would lead to an increase in precipitation from September to February and a notable decrease from May to August. According to their results, mean annual streamflow would increase by 10% (A2 scenario) or 6.4% (B2 scenario) by the end of the century. However, according to Girvetz et al. (2012) knowing how temperature and precipitation is projected to change on average in the future is not very useful for decision support. Instead, precipitation and temperature changes must be used to create more adapted applications and information indicating the corresponding impacts on water supply, biodiversity, agriculture, and more. There is a need to deliver this data in a comprehensible format and with understandable conclusions to decision-makers, planners, and engineers.

2. Study area

The upper BNB is located in the northwestern part of Ethiopia; it is the largest tributary of the Nile River and covers a drainage area of 175,000 km^2. Its extent goes from the escarpment of the Rift Valley in the east to the Sudanese border in the west and from Lake Tana in the North down to Ambo (see Figure 1). The upper BNB covers 17% of Ethiopia's surface area, generates 43% of the country's total average runoff, and is home to about 25% of its total population (Taye and Willems, 2012). The BNB's elevation ranges from 350 m asl near the Sudanese border to

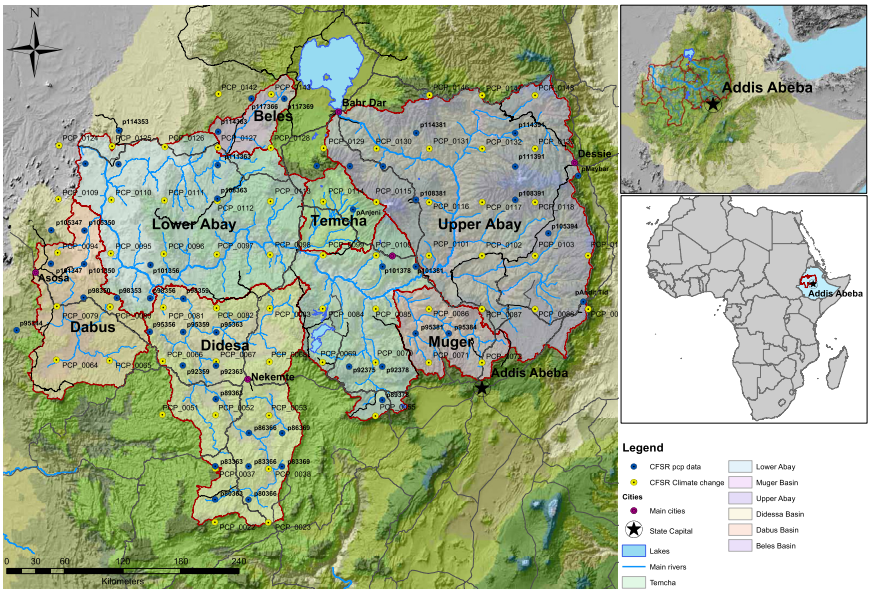

Figure 1. Map overview of upper Blue Nile (Abay) Basin with CFSR climate stations, climate change stations, and agro-ecological zones according to Hurni (Hu et al., 2007).

4,230 m asl in the central part of the basin (Betrie et al., 2011; Taye et al., 2015). The climate of the basin varies significantly according to the altitude and is governed by the seasonal migration of the Inter-Tropical Convergence Zone, or ITC (Mccartney et al., 2012). Annual rainfall varies from 400 mm near the Ethiopia–Sudan border to 2,200 mm in the Didesa and Dabus sub-basins. The eastern part of the BNB has a bimodal rainfall regime with the short rainy season (*belg*) lasting from February to May and the long rainy season (*kremt*) lasting from June to September. The western part of the BNB has a unimodal rainfall regime with the kremt lasting from June to September. The Blue Nile River discharge regime is highly seasonal with over 80% of its annual discharge occurring from July to October, and only 4% from January to April (Kim and Kaluarachchi, 2009; Sutcliffe and Parks, 1999). The upper BNB contributes roughly from 60 to 70% of the total annual flow component of the main Nile (Nawaz et al., 2010).

2.1. Sub-basins of the Abay Basin

This section briefly describes the eight sub-basins used to model the upper Blue Nile Basin in this study. Each sub-basin was defined according to certain criteria dictated by data availability and locations of discharge and rainfall measuring stations. Although the Lake Tana sub-basin is part of the Abay basin, it was not considered for modelling because of its many irrigation schemes and because of the water abstraction via the Lake Tana–Beles hydropower scheme (Haile et al., 2009). As no data were available for modelling the Lake Tana sub-basin, the present research

focuses on the Blue Nile river from the outlet of Lake Tana to the Sudanese border (see Figure 1 for details).

The Beles sub-basin

The Beles sub-basin is by far the smallest sub-watershed of the Abay. The elevation ranges from 944 m asl up to 2736 m asl over an area of 3526 km^2. It is located at the northern end of the Abay, southwest of Lake Tana. The Beles sub-basin contributes roughly 1.5% (mean contribution, 1989–2002) of the total outflow of the Abay River at the lower Abay outflow.

The Kessie sub-basin

Approximately 48,961 km^2 with a range extending from 1011 m asl to 4245 m asl make up the Kessie sub-basin. The Kessie sub-basin was given by the availability of discharge data between Lake Tana and the Kessie Bridge. No data on large tributaries or data on the Blue Nile River were available in between. Consequently, the sub-basin was modelled as seen in Figure 1. Climate Forecast System Reanalysis (CFSR) data were used for simulation (1979–2013), as were available rainfall data from the Water and Land Resource Centre (WLRC) covering the eastern parts of the basin from 1981 to 2013. The Kessie watershed contributes roughly 35% streamflow to the Abay Basin and is computed using the Lake Tana sub-basin as inlet.

The Temcha sub-basin

The Temcha basin is located at the centre on the north side of the Abay basin and covers an area of 5,526 km^2 with an altitudinal range extending from 748 m asl up to 4088 m asl. Rainfall data from WLRC and from CFSR were used for simulation. The Temcha sub-basin contributes an average of 2.4% to the total outflow of the Abay Basin.

The Muger sub-basin

The Muger sub-basin is located to the southeast of the Abay Basin. Studies (Azagegn et al., 2015; Berehanu et al., 2017) show that the aquifer system is connected to the upper Awash basin, which drains towards the southeast. This singularity combined with a lack of data makes calibration of the Muger basin very difficult. On average, the mean contribution of the Muger sub-basin is 0.97%.

The Didesa sub-basin

The Didesa sub-basin is on the south-westerly side of the Abay Basin and has the second-largest area of the sub-basins covering roughly 28,189 km^2. The Didesa

 https://doi.org/10.1016/j.heliyon.2018.e00771

sub-basin ranges form 609 m asl up to 3210 m asl. On average the Didesa sub-basin contributes 10.9% to the outflow of the Blue Nile.

The Dabus sub-basin

The Dabus sub-basin is located at the westernmost side of the Abay basin and covers an area of approximately 14,741 km^2. Its elevation ranges from 467 m asl to 3130 m asl. It drains northwards into the lower Abay and displays the highest mean rainfall in the basin (2200 mm). This high mean annual rainfall is reflected in its high contribution to the total Blue Nile flows. On average, the Dabus sub-basin contributes 20.8% to the total outflows.

The Lake Tana sub-basin

Running from the source of the Abay to Lake Tana, this sub-basin is dominated by several hydropower schemes, one of which is the Tana–Beles hydropower plant. However, since the water outtake could not be reliably modelled, the present study omits the Lake Tana basin and instead uses discharge data from Lake Tana (1982–2010) as inflow data to the Kessie sub-basin.

The lower Abay sub-basin

The lower Abay sub-watershed is the largest watershed in the research area. It spans from the Kessie Bridge down to the Sudanese border. The lower Abay sub-watershed was simulated with inlets from the six other sub-basins described above. On average, the lower Abay watershed receives 77% of the streamflow from above and contributes roughly 23% from its surface. Further, an annual average of 1,734.5 cubic meters per second (cms or m^3/s) flow out of the sub-basin, with the peak outflow occurring in August at about 6,147 cms and the lowest outflow occurring in March at about 225.7 cms. The mean yearly contribution of the entire upper Abay basin is 54,697,000,000 m^3 or 54.6 km^3.

3. Materials & methods

The Soil and Water Assessment Tool (SWAT) is a physically based, spatially distributed, continuous-time hydrological model used to simulate continuous-time landscape processes at the catchment level (Arnold et al., 1998; Neitsch et al., 2011).

Using SWAT, the research catchment is divided into lumped non-spatial hydrological response units (HRUs), which are units with similar soil types, land use, and slope classes. The model uses HRUs to describe spatial heterogeneity in a watershed. The major model components include hydrology, climate and weather,

 https://doi.org/10.1016/j.heliyon.2018.e00771

erosion/sedimentation, plant growth, nutrients, pesticides, land management, and stream routing. The model predicts hydrology at each HRU using the following water balance equation (Arnold et al., 2011; van Griensven et al., 2012)

$$SW_t = SW_0 + \sum_{i=1}^{t}(R_{day} - Q_{surf} - E_a - W_{seep} - Q_{gw}) \quad (1)$$

The SWAT model includes sub-basins, reservoirs, and channel-routing components. The sub-basin component simulates runoff, erosion, soil water movement, evapotranspiration, crop growth and yield, soil nutrient and carbon cycling. The reservoir component detains water, sediment, and pollutants. Finally, the channel component routes flows and sediments and degrades nutrients, pesticides, and bacteria during transport (Douglas-Mankin et al., 2010).

3.1. Model input

In order to run the SWAT model, it was necessary to prepare several sets of spatially distributed data. The ArcSWAT interface requires a Digital Elevation Model (DEM), soil data, land use data, and rainfall data including climate data (see Table 3 on page 15 for details). Finally, measured rainfall and streamflow data were used for calibration and validation. The availability of streamflow data was decisive regarding the final definition of sub-basins for use in our model. The upper Blue Nile was divided into seven sub-basins according to the availability of streamflow data (see Figure 1 for details).

3.1.1. DEM

Topography was defined using a Digital Elevation Model (DEM) with a 30 × 30 m resolution from the Advanced Spaceborne Thermal Emission and Reflection Radiometer (ASTER). The DEM is used to delineate the watershed and to analyse drainage patterns. The river network was created using the ArcGIS interface and was validated by means of existing river networks derived from satellite images and by means of ground-truthing during fieldwork. The DEM was further used to define slope gradients; slope length; channel slope, length, and width; and sub-watersheds.

3.1.2. Land use and soil data

The initial land use and land cover data sets obtained were produced at a spatial resolution insufficient for the requirements of this study and were not related to topography. The Global Land Cover Characterization (GLCC) database of the

 https://doi.org/10.1016/j.heliyon.2018.e00771

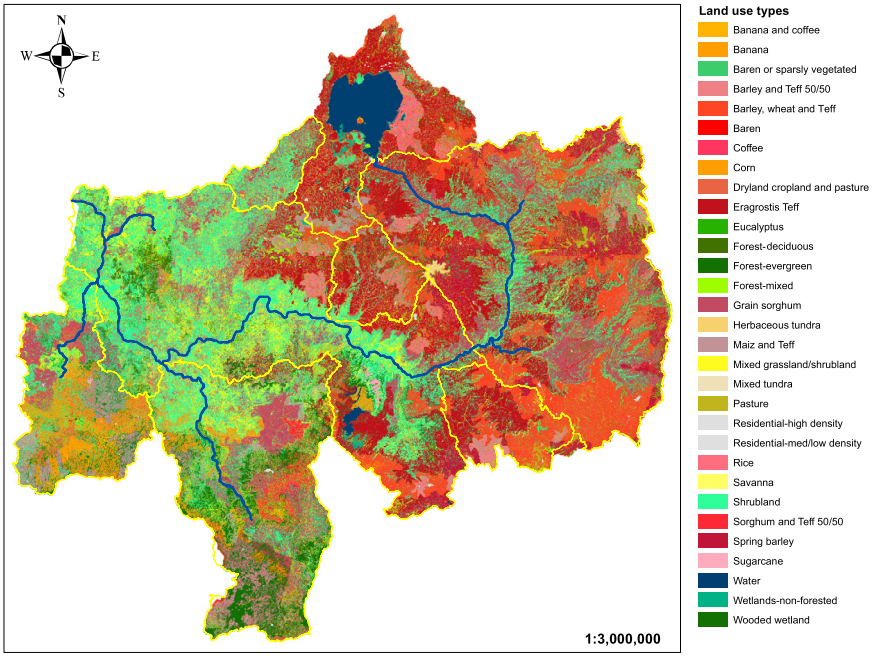

Figure 2. Map overview of land use layer for SWAT.

United States Geological Survey (USGS) is produced at a resolution of 1 km (Ali, 2014), while the map from the Eastern Nile Technical Regional Office (ENTRO) only has five dominant land use categories (Easton et al., 2010) and the BCEOM only has seven land cover categories (Dessie et al., 2014). High-resolution land use maps were only available for small watersheds within the target area, such as, for example, the high-resolution land use maps of the WLRC (Setegn et al., 2010). Thus, Kassawmar et al. (2016) developed a land cover dataset for the Ethiopian Highlands featuring a resolution of 30 m (for details, see the Economics of Land Degradation [ELD] Ethiopia Case Study from Hurni et al., 2015). For the present study using SWAT, additional land use classes were needed to represent the system. Thus, new land use classes were added to the ELD classes by incorporating two additional datasets: (1) the FAO's farming and cropping system and livelihood zone map (Medhin, 2011); and (2) the agro-ecological zone maps of Hurni (1998) with integrated local knowledge from local partners (see Figure 2 and Table 1 for details).

Similarly, soil maps were combined from different sources and reclassified for better integration into the SWAT model. For this purpose, soil maps from Brunner (2012) with a soil topography relationship were reclassified with the superordinate soil categories containing more specific soil categories from the Harmonized World Soil Database (HWSD). Reclassification was performed based on spatial and geomorphological conditions of the different soil types. This made it possible to link the HWSD soil classes with the soil parameters of the SWAT database (see Figure 3 and Table 2 for details).

https://doi.org/10.1016/j.heliyon.2018.e00771

Table 1. Land use/land cover types and coverage.

SWAT land use type	WLRC land use classes	Crop rotation (OpSchedule)	BNB Area [km^2]	BNB % of total area
SHRB	Shrubland	AGRR	37,355.16	21.43
TEFF	Eragrostis Teff	TEFF/TEFF1	22,777.23	13.07
CRDY	Dryland cropland and pasture	AGRR	16,453.89	9.44
BWTF	Barley, Wheat and Teff	BARL/BARL1	15,841.12	9.09
GRSG	Grain Sorghum	CORN/CORN1	13,225.73	7.59
MIGS	Mixed Grassland/Shrubland	AGRR	12,212.19	7.01
FRSE	Forest-Evergreen	FRSE	8,694.52	4.99
BARL	Spring Barley	BARL/BARL1	6,057.46	3.48
BARR	Barren	SWRN	5,895.60	3.38
CORN	Corn	CORN/CORN1	5,288.42	3.03
FRST	Forest-Mixed	FRST	4,812.12	2.76
COTF	Maiz and Teff	CORN/CORN1	4,540.01	2.60
PAST	Pasture	PAST	4,040.28	2.32
WATR	Water	WATR	3,364.04	1.93
BSVG	Baren or sparsely vegetated	SEWN	2,896.77	1.66
BATF	Barley and Teff 50/50	TEFF/TEFF1	2,559.19	1.47
FRSD	Forest-Deciduous	FRSD	2,171.62	1.25
EUCA	Eucalyptus	FRST	1,320.57	0.76
SGTF	Sorghum and Teff 50/50	TEFF/TEFF1	1,141.82	0.66
RICE	Rice	RICE	799.52	0.46
SAVA	Savanna	AGRR	618.15	0.35
COFF	Coffee	AGRR	555.57	0.32
WETN	Wetlands-Non-Forested	WETN	490.08	0.28
TUHB	Herbaceous Tundra	AGRR	314.09	0.18
CPNM	Residential-Med/Low Density	AGRR	284.95	0.16
SUGC	Sugarcane	AGRR	152.56	0.09
URHD	Residential-High Density	AGRR	143.42	0.08
WEWO	Wooded Wetland	FRSE	112.86	0.06
TUMI	Mixed Tundra	FRSE	76.83	0.04
BANA	Bananas	AGRR	59.60	0.03
BACO	Banana and coffee	AGRR	31.69	0.02
Total			174,287	100

3.1.3. Hydrometeorologic and climatic data

Data required for this study were compiled from various sources. The hydro-meteorological data (daily precipitation, maximum and minimum temperature, daily solar radiation and wind) were obtained from: (1) the WLRC in Addis Abeba; (2) the National Meteorological Agency (NMA) of Ethiopia; and (3) the Climate Forecast System Reanalysis (CFSR) of the National Centres for Environment Prediction (NCEP).

CFSR rainfall and climate data were obtained via the Texas A&M University (TAMU) Spatial Science website (globalweather.tamu.edu; *accessed October 2015*) for the entire Abay basin (bounding box: latitude 8.60°–12.27° N and longitude 33.94°–40.40° E). Rainfall and climate data were obtained from the NMA in Addis Abeba. The NMA dataset comprised 35 meteorological stations and time series from 1970 to 2004, but contained significant gaps. In order to identify the most accurate rainfall and climate stations out of the 399 CFSR stations, they were correlated to

 https://doi.org/10.1016/j.heliyon.2018.e00771

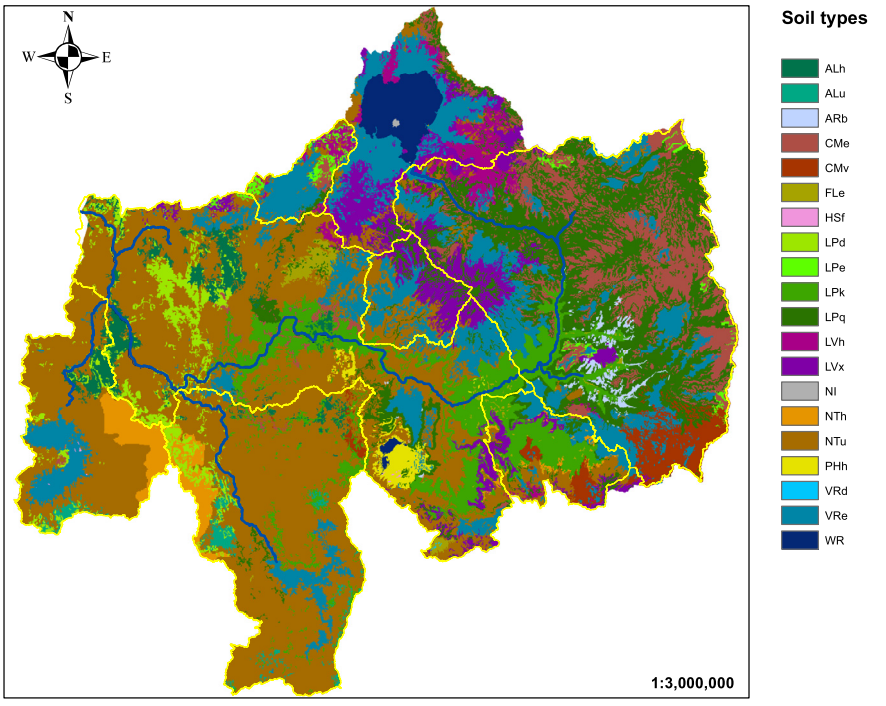

Figure 3. Map overview of soil types layer for SWAT and sub-basin layer.

Table 2. Soil types in the Abay Basin.

SWAT land use types	WLRC land use classes	BNB Area [km^2]	BNB % of total area
NTu	Humic Nitisols	64,578	35.99
VRe	Eutric Vertisols	24,751	14.46
LPq	Lithic Leptosols	24,496	14.32
LPk	Rendzic Leptosols	13,344	7.80
CMe	Eutric Cambisol	12,797	7.48
LVx	Chromic Luvisols	9,544	5.58
LPd	Dystric Leptosols	4,516	2.64
ALh	Haplic Alisols	3,790	2.22
CMv	Vertic Cambisols	3,739	2.19
LVh	Haplic Luvisols	3,670	2.15
NTh	Haplic Nicisols	3,370	1.97
PHh	Haplic Phaeozems	1,324	0.77
FLe	Eutric Fluvisols	1,115	0.65
ALu	Humic Alisols	1,092	0.64
LPe	Eutric Leptosols	1,055	0.62
ARb	Cambic Arenosols	900	0.53
HSf	Fibric Histosols	24	0.01
VRd	Dystric Vertisols	9	0.01
Total		171,122	100

NMA and WRLC climatic stations in the respective sub-basins. Time series were compared for mean monthly rainfall and for seasonal lows and peaks. Goodness of fit was determined through the Root Mean Square Error-observations standard deviation ratio (RSR), the Nash–Sutcliffe Efficiency (NSE), and the percent Bias

 https://doi.org/10.1016/j.heliyon.2018.e00771

(PBIAS) while also monitoring ME, R2, skewness, standard deviation as well as the number of recorded years and mean yearly rainfall. Of the initial 399 CFSR stations covering the entire BNB, a total of 42 were retained for SWAT simulations because their data significantly correlated with measured NMA and WLRC data (see Figure 1 for details).

3.1.4. Discharge data

There are relatively few reliable hydrologic stations in the Abay Basin, despite its size. This is mainly due to general inaccessibility, remoteness, and economic constraints on setting up and maintaining adequate monitoring networks (Kim and Kaluarachchi, 2008). Thus, for the present study, river discharge data were obtained from different sources. Daily discharge data were obtained from the International Water Management Institute (IWMI) of the Hydrology Department of the Ministry of Water Resources of Ethiopia, and from the WLRC in Ethiopia. The sub-basins in the SWAT were designed to fit the available hydrological stations (see Figure 1 for details). Still, the available discharge data were characterized by significant gaps, occasional extremes for no apparent reason, and missing data. Thus, whenever possible, the apparently unreliable stations were removed and sub-basins were modelled using the most reliable data sources possible.

3.2. Climate change data

The CFSR data from 1979 to 2013 were adopted as the baseline climate scenario for the Abay Basin, indicating typical precipitation and temperature patterns. Three General Circulation Models (GCM) were used to model future climate change. The CGCM 3.1 (Canadian Global Coupled Model 3.1) from the Canadian Centre for Climate Modelling and Analysis (CCCMA), the CNRM-CM 3 (Salas-Mélia et al., 2005) from the Centre National de Recherches Meteorologiques (CNRM), and the MRI-CGCM 2.3.2 from the Meteorological Research Institute, Japan Meteorological Agency, were applied on behalf of two future simulation periods: 2046–2064 (mid-century) and 2081–2099 (end of century).

Three different GCMs were used because it is typically difficult to select a specific GCM for a given study area. The precipitation and temperature files for the simulation periods were acquired in SWAT file format from the Climate Change Data for SWAT website (CMIP3, cmip.tamu.edu/cmip, unfortunately this website is not currently online). This website makes downscaled and bias-corrected data available that span the entire globe and have been generated through a collective effort between The World Bank, The Nature Conservancy, Climate Central, and Santa Clara University, USA (Girvetz et al., 2012). Additionally, each GCM corresponds

with different scenarios of future development. Each scenario represents a specific quantification of one of four possible "storylines". For the present research, the A1B scenario was used: it posits a future world featuring rapid economic growth, a global population that peaks by mid-century (2050) and declines thereafter, and the rapid introduction of new and more efficient technologies. Under the A1B scenario, the technological emphasis is balanced across all energy sources (IPCC, 2000), i.e. no one particular energy source is relied upon. Storylines A2 (self-reliance and preservation), B1 (service and information economy), and B2 (environmental protection and social equity) were rejected for credibility reasons.

3.2.1. Climate change in the Abay Basin

Under the IPCC A1B scenario the three models (CCCMA, CNRM, MRI) show similar trends for temperature change for both of the two chosen periods (2046–2064 and 2081–2099). The absolute temperature change varies from +2.0 °C (10.3%) to +2.7 °C for the mid-century period and from +2.7 °C to +3.7 °C (18.8%) for the end of century period for the Abay Basin (see Table 9 on page 21 for details). All GCMs show that the mid-century significantly deviates from the baseline but the end of century projection will generally increase but to a lesser extent than the mid-century temperature from the baseline (see Figure 4 on page 14 for details).

All GCMs project a general temperature increase with a more or less significant loss of seasonality. The CCCMA and MRI models show a small variation of mean monthly temperature throughout the year (±4 °C) and do not show the temperature drop from June to September, which is consistent with the projected rainfall pattern. The CNRM model projects a strong increase of temperature from January to April and a significant drop in mean temperature after May.

Under the A1B scenario, the three GCMs display similar patterns of precipitation change over the upper Abay basin. All three GCMs showed that changes in precipitation will not only affect the mean total yearly amount of rainfall (changes from +17.7% to +46%) but will also impact the annual rainfall distribution (see Figure 4 for details). All three GCMs point to an increase in mean annual precipitation (varying from +241 mm to +639 mm for the mid-century period, see Table 7 on page 20 for details).

The end of century period shows a further increase in mean annual precipitation for the CNRM and the MRI models going from +381 mm (+27%) to +671 mm (+48%). The CCCMA model projects a decrease from mean annual mid-century rainfall to +7% from baseline. All GCMs show a similar trend regarding the annual distribution of rainfall (see Figure 4 for details). For the mid-century period peak mean monthly precipitation is reduced but the duration of the rainfall period is extended to before

 https://doi.org/10.1016/j.heliyon.2018.e00771

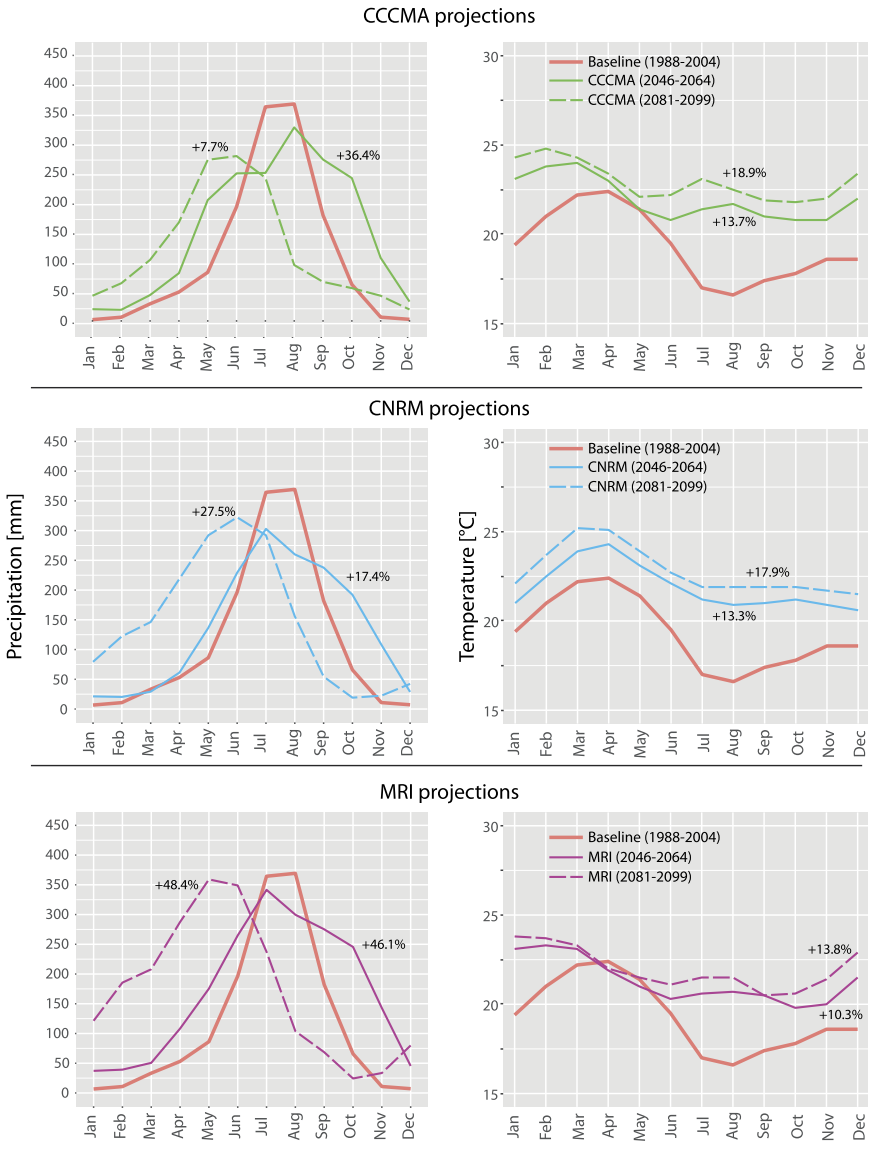

Figure 4. Mean monthly precipitation and mean monthly temperature for the Upper Blue Nile Basin. Shown here are the baseline from 1979 to 2013 (red) as well as the two projected periods (2046–2064 and 2081–2099) for each GCM. The numbers give the percentage change to the baseline.

and after the baseline rainfall period (January to May and September to December, respectively).

The end of century period shows a reduced increase in precipitation compared to the baseline for the CCCMA projection and further increases for the CNRM and the MRI projections. All projections display a clear decline in seasonal rainfall during the main rainy season, with rainfall shifting to earlier months in the year and a longer duration of the rainfall season (January to September) and generally lower monthly peaks throughout the year.

Table 3. Spatial model input data and sources.

Data type	Description	Resolution	Source
Topography map	Digital Elevation Map (DEM)	30 m	SRTM
Land use map	Land use classification	30 m	CDE-WLRC
Soil map	Soil types map	30 m	CDE-WLRC
Weather data	Daily precipitation Daily temperature	0.25° × 0.25°	NCEP/NCAR
	Daily precipitation Daily temperature	3 stations	SCRP/WLRC
Hydrology data	monthly discharge	12 stations	MoWE
Climate Change	CCCMA-CGCM3.1	0.5° × 0.5°	SWAT
	CNRM-CM3	0.5° × 0.5°	SWAT
	MRI_CGCM2.3.2	0.5° × 0.5°	SWAT

Table 4. Initial parameter range and final calibrated values for subwatersheds.

	Initial value	Beles	Dabus	Didesa	Muger	Temcha	Kessie	Lower Abay
CN2	0	−12 to 4	−6 to 6	−6 to 5	−9 to 9	−5 to 10	−8 to 10	−10 to 10
GW_DELAY	0 to 500	0 to 80	60 to 100	40 to 250	10 to 400	5 to 100	1 to 60	10 to 350
GWQMN	0 to 5000	3000 to 5000	2000 to 2500	1000 to 3500	3000 to 5000	2000 to 5000	100 to 4000	3500 to 5000
GW_REVAP	0.02 to 0.2	0.15 to 0.2	0.05–0.08	0.17 to 0.19	0.19 to 0.2	0.07 to 0.2	0.03 to 0.19	0.17 to 0.2
REVAPMN	0 to 500	1 to 210	50 to 100	10 to 85	50 to 300		1 to 350	50 to 400
CH_K2	−0.01 to 500	0 to 300	100–300	10 to 190	200 to 500	0 to 100	0 to 200	150 to 400
RCHRG_DP	0 to 1	0 to 0.3	0 to 0.1	0.1 to 0.6	0.01 to 0.1	0.01 to 0.2	0 to 0.3	0 to 0.2
SOL_AWC	−0.5 to 0.5	0 to 1	0.02 to 0.1	0.2 to 0.9	0 to 2	0.1 to 0.7	0.1 to 0.7	0 to 2
CH_N2	−0.01 to 0.3	0.01 to 0.25	0.05 to 0.15	0.075 to 0.5	0.05 to 0.15	0.05 to 0.15	0.03 to 0.15	0.05 to 1.5
ALPHA_BF	0 to 1	0.2 to 0.7	0.07 to 0.1	0.1 to 0.6	0.1 to 0.5	0.75 to 0.95	0.1 to 0.8	0.6 to 1
SOL_K	0 to 2000	−0.5 to 2	0.4 to 0.8	0.75 to 1.8	0 to 2	0 to 2	0–2	0 to 2

4. Methodology

The SWAT model was set up using the ASTER Digital Elevation Model with a resolution of 30 × 30 m. Sub-basin partitioning and stream networks were first computed automatically with ArcSWAT, and then adapted to the outlet feature classes to reflect the available river gauges (see Figure 1). Each of the six upstream watersheds (Beles, Kessie, Temcha, Muger, Didesa, and Dabus) was calibrated individually using the baseline climate data and the available streamflow data. Each watershed was then run for the entire period from 1979 to 2014 using the calibrated parameter settings. This final run from each sub-basin was then used as an inflow data to the lower Abay watershed during its calibration run. Each watershed was calibrated using 500 simulations for each iteration. Initial parameter range values were set at the same absolute magnitude for each sub-basin (see Table 4 for details).

After calibration and validation, each of the seven upstream watersheds was run once with the best simulation parameters using the climate change rainfall and temperature data from CMIP3. Thus, each watershed was run for three different GCMs and each GCM was run for scenarios A1B. Each scenario for each GCM was compared and analysed regarding outcomes according to scenarios A1B (see subsection 3.2.1 for details on A1B).

 https://doi.org/10.1016/j.heliyon.2018.e00771

4.1. Model performance evaluation

The seven watersheds were calibrated using SWAT-Cup (Abbaspour, 2005, 2015; Abbaspour et al., 2007) while using model performance ratings from different sources. The model evaluation was first performed using calibration techniques suggested by Abbaspour (2015) and Arnold et al. (2012) for the *p-factor* and the *r-factor* before statistically rating the performance as recommended by Moriasi et al. (2007), Van Liew et al. (2007), and Saleh et al. (2000) The goodness of fit was determined by the coefficient of determination (R^2), the Nash–Sutcliffe efficiency (*NSE*), the ratio of the root mean square error (RMSE) between simulated and observed values to the standard deviation of the observations (RSR), and the coefficient of determination multiplied by the slope of the linear regression between simulation and observation (bR^2, Krause et al., 2005).

The *p-factor* is the percentage of observed data enveloped by the modelling result, also known as the 95 percent prediction uncertainty (95PPU) while the *r-factor* is the relative thickness of the 95PPU band (see Abbaspour et al., 2004, and Schuol et al., 2008, for details). Depending on the quality of measured data the *p-factor* should range around 0.60 while the *r-factor* should be <1.3. Once *p-factor* and *r-factor* are satisfactory model performance can be statistically evaluated using R^2, NSE, bR^2, and RSR.

5. Results & discussion

This section first discusses the calibration and performance ratings of the sub-watersheds of the upper Abay basin before presenting the results of applying climate change data to the calibrated model.

5.1. Subwatershed calibration and validation

Six sub-basins of the upper Abay were calibrated individually and their calibrated outflows were used as inflows for the lower Abay basin (see Figure 6 for details). The calibration of the six sub-watersheds performed satisfactorily to very good. Larger sub-watersheds performed better than smaller ones. The lower performance of the Muger sub-watershed could be due to the above-mentioned loss of water via the aquifer connection between the Muger and the Awash basin, which could not be accounted for. The Muger sub-watershed had long periods of low flows that could not be calibrated using this parameter setup, and the model could not be further adapted due to lack of reliable information. Nonetheless, the model performed well overall (see Tables 4 and 8 respectively), as indicated by the good results of R^2, NSE,

 https://doi.org/10.1016/j.heliyon.2018.e00771

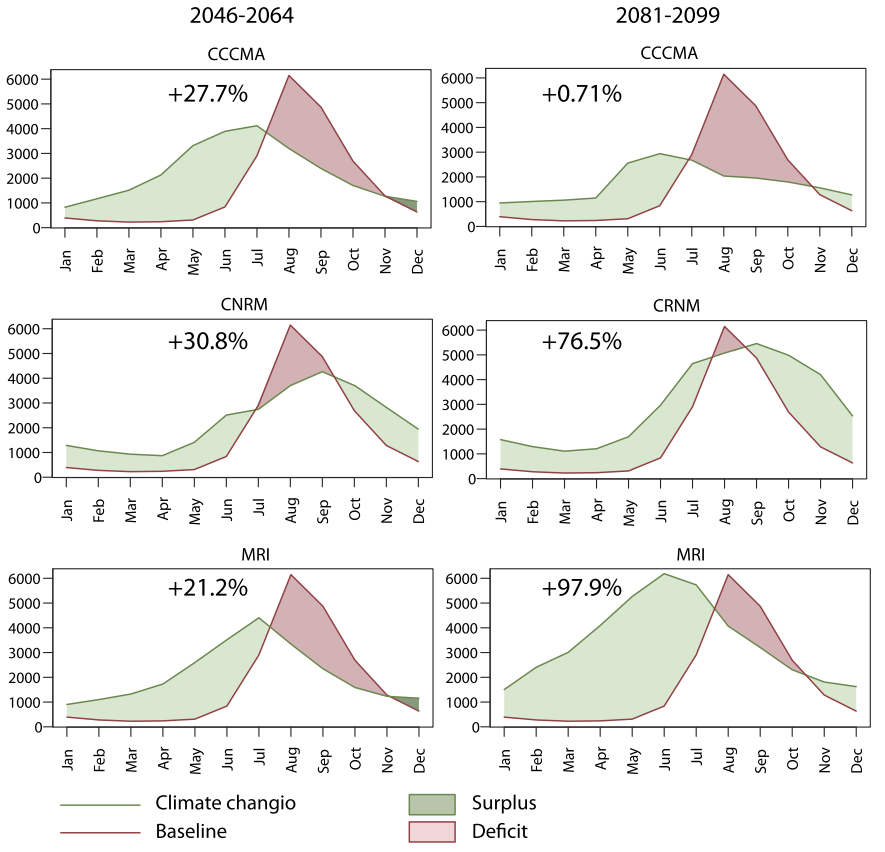

Figure 5. Mean monthly outflow in m^3/s for the upper Blue Nile Basin at the border to Sudan. Shown here are the baseline in red, the outflow under climate change scenario as well as a surplus and deficit where applicable. The numbers indicate the percentage change to baseline outflow.

bR^2, and RSR (see section 4.1 for details on model performance as well as Table 8 for calibration and validation results).

5.2. Application of climate change data

The streamflow of the Abay basin is composed of six inflows from upstream watersheds (see Figure 1 for details). These watersheds were used to generate the total outflow from the Lower Abay basin and the total outflow of the upper Blue Nile Basin. The results are divided according to the two projected periods in the 21st century.

The upper Abay Basin from 2046 to 2064

Application of the three GCM models to the SWAT points to a shift away from the current main outflow season towards an earlier peak (temporally) and a longer, more gradual extension of annual outflow (see Figure 5 for details). Generally, an increase

 https://doi.org/10.1016/j.heliyon.2018.e00771

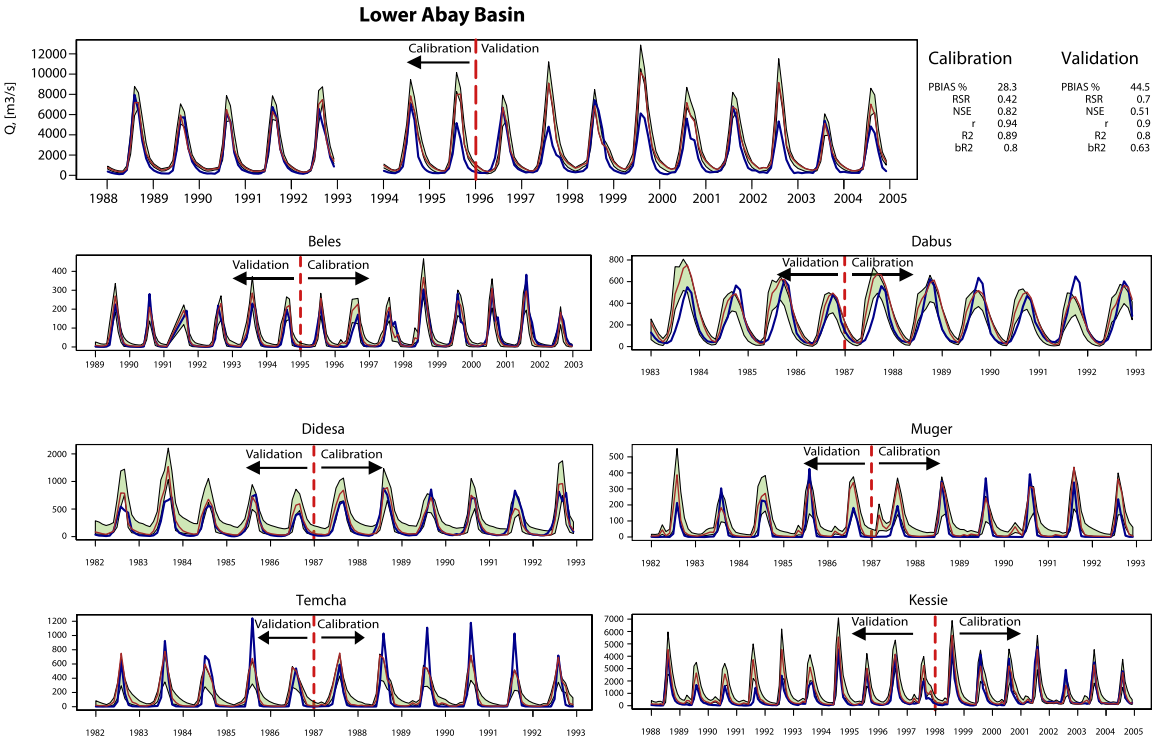

Figure 6. Graphical overview of calibration and validation results for all sub-basins. Calibration statistics are given in Table 8 on page 21.

of between 21% and 30% is projected over the current outflow, which presently stands at 1,734 m^3/s. The CCCMA and the MRI model both project a strong increase in flows from January to June with an equally strong decrease for the period June to November. The CNRM model projects a shift in the main rainy season moving it towards the end of the year with a peak in September and a higher distributed outflow throughout the year. All projected outflows follow their respective projected rainfall pattern regarding seasonality. This means that streamflow shifts in the same direction as projected rainfall shifts. Regarding rainfall amounts and rainfall amount changes, the relationship to streamflow is less apparent. The CCCMA model estimates that mean average yearly rainfall will increase approximately 36%, resulting in a streamflow increase of 27% at the outflow of the Abay river. The CNRM model projects an increase of 17.4% in mean annual precipitation, resulting in a streamflow increase of 30%. Finally, the MRI model projects an increase of 46% in mean annual precipitation, resulting in an increase of mean streamflow of 21.2%.

The upper Blue Nile Basin from 2081 to 2099

Application of the climate change scenarios for the period at century's end revealed a more pronounced change in outflows from the upper Abay basin. The CCCMA

Table 5. Mean monthly outflow in cubic meters per seconds (CMS) at the outflow of the upper Blue Nile Basin.

	Baseline (1988–2004)	CCCMA	CNRM	MRI	CCCMA	CNRM	MRI
		(2046–2064)			(2081–2099)		
Jan	1015.40	824.60	1286.50	902.90	947.80	1576.50	1504.20
Feb	757.41	1167.00	1067.90	1100.60	1007.20	1293.20	2403.80
Mar	555.08	1512.80	931.90	1325.00	1061.80	1109.40	3008.80
Apr	514.26	2129.00	871.00	1728.70	1147.50	1207.00	4092.00
May	613.17	3313.90	1410.60	2597.40	2557.60	1692.30	5264.40
Jun	1048.99	3892.10	2510.50	3516.20	2940.50	2967.00	6186.70
Jul	3682.00	4118.10	2743.80	4404.70	2677.60	4645.60	5733.70
Aug	7303.94	3196.70	3700.10	3344.20	2037.00	5072.70	4069.60
Sep	6204.25	2393.10	4264.10	2346.80	1955.50	5456.30	3204.30
Oct	3346.12	1704.40	3668.20	1588.50	1796.90	4985.90	2302.80
Nov	2114.56	1269.30	2822.00	1233.00	1560.00	4199.50	1809.90
Dec	1449.50	1061.40	1942.70	1153.10	1272.80	2534.10	1623.20
Mean	1734.70	2215.20	2268.30	2103.40	1746.80	3061.60	3433.60
Abs. diff. [cms]		480.50	533.60	368.70	12.10	1326.90	1698.90
Rel. diff [%]		27.70	30.80	21.30	0.70	76.50	97.90

Table 6. Baseline and projected outflow from the Upper Blue Nile Basin. The long-term mean Nile flow is given as 80 $km^3\ y^{-1}$ and is taken from Siam and Eltahir (2017).

	Baseline (1988–2004)	CCCMA	CRNM	MRI	CCCMA	CRNM	MRI
		(2046–2064)			(2081–2099)		
Mean annual cms [$m^3\ s^{-1}$]	1734.72	2203.09	2269.01	2102.48	1747.03	3061.78	3433.01
Annual outflow [$km^3\ y^{-1}$]	54.7	69.5	71.6	66.3	55.1	96.6	108.3

model projects an increase in mean annual precipitation of +7%, resulting in an increased annual outflow of +0.7%, coupled with a strong temporal shift away from the baseline rainy period. The CNRM model projects an increase in mean annual precipitation of +27%, resulting in a mean monthly streamflow increase of +76%. The predicted streamflow is mainly distributed around the baseline peak period, accompanied by a prolonged outflow increase between May and December and generally increased streamflow between January and May (see Table 5 for details). The MRI model projects an increase of 48% in mean annual precipitation, coupled with a clear temporal shift in rainfall towards the beginning of the year, peaking in April. This leads to a strong increase in streamflow (+97%) between January and May, followed by a slow decrease through November before starting again in December (see Table 5 for details).

The upper Blue Nile flows in the Nile Basin

According to Siam and Eltahir (2017), the long-term flows of the Nile (1900–2000) are approximately 80 $km^3\ y^{-1}$; they project these flows to increase to 92 $km^3\ y^{-1}$ by the end of the 21st century (see Table 6 for details).

In the present study, Abay basin baseline outflows from the calibrated SWAT model were compared with projected outflows after applying the three GCMs for the two

 https://doi.org/10.1016/j.heliyon.2018.e00771

Table 7. Weighted mean precipitation for the Blue Nile Basin from baseline (1988–2004) to projection 1 (2046–2064) and projection 2 (2081–2099).

	Baseline	CCCMA 1	CCCMA 2	CNRM 1	CNRM 2	MRI 1	MRI 2
Jan	6.67	24.30	46.86	21.28	79.36	37.19	121.36
Feb	10.79	23.27	67.87	20.33	122.24	39.23	185.57
Mar	33.31	48.04	107.24	29.17	146.31	50.65	208.05
Apr	53.14	84.84	170.20	61.35	219.17	108.31	287.48
May	86.21	207.77	275.39	136.54	292.08	175.37	359.10
Jun	196.50	252.62	281.75	229.17	322.34	264.88	348.95
Jul	364.42	253.32	245.28	305.95	292.13	341.58	237.31
Aug	369.33	329.91	98.53	260.05	155.92	299.71	103.86
Sep	182.18	275.90	70.20	237.77	54.53	275.18	68.56
Oct	65.86	244.68	59.68	192.13	19.11	245.58	24.36
Nov	10.87	110.53	46.87	108.49	22.41	142.85	33.55
Dec	7.16	37.00	23.76	28.76	42.29	45.42	79.89
Sum	1386.45	1892.19	1493.64	1627.99	1767.90	2025.94	2058.04
Abs. diff. (mm)		505.74	107.19	241.54	381.45	639.49	671.58
Rel. diff. (%)		36.48	7.73	17.42	27.51	46.12	48.44

reference periods. The calibrated SWAT model for the Abay basin indicates an annual outflow of 54.7 $km^3\ y^{-1}$, which is approximately 68% of the total Nile flow of 80 $km^3\ y^{-1}$. The CCCMA model projects an increase in Abay basin outflow to as high as 69.5 $km^3\ y^{-1}$ for the mid-century period, followed by a decline back down to 55.1 $km^3\ y^{-1}$ for the period at century's end. The CNRM model projects an increase to as high as 71.6 $km^3\ y^{-1}$ for the mid-century period, followed by an additional increase to as high as 96 $km^3\ y^{-1}$ for the period at century's end. The MRI model projects an increase to 66.3 $km^3\ y^{-1}$ around mid-century, followed by another increase to arrive at outflows as high as 108 $km^3\ y^{-1}$ (roughly double the baseline) for the period at century's end.

5.3. Uncertainty of climate change application and of ensuing impacts on streamflow

Hydrological modelling virtually always contains uncertainty. This stems in particular from (1) the uncertainty of recorded field data (Abbaspour et al., 1997), and (2) the uncertainty of the applied hydrological model itself (Adem et al., 2016). When applying climate change models, additional uncertainties are introduced including that of (3) the internal variability of the climatic system, (4) the development of the climatic system, and (5) the implementation of these changes within the GCM and the technique used for downscaling (Bates et al., 2008). In this way, the present research has clear limitations. Each of the above sources of uncertainty applies, and not all of them can be quantified. Thus, the results should be treated with appropriate caution.

 https://doi.org/10.1016/j.heliyon.2018.e00771

Table 8. Calibration and validation statistics for the upper Blue Nile Basin.

Sub-basin	P-factor		R-factor		R^2		NSE		bR^2		RSR	
	Cal	Val	Cal	Val	Cal	Val	Cal	Val	Cal	Val	Cal	Val
Beles	0.78	0.83	0.67	0.69	0.85	0.90	0.83	0.86	0.84	0.83	0.40	0.40
Dabus	0.64	0.65	0.75	0.92	0.76	0.75	0.66	0.45	0.70	0.61	0.50	0.50
Didesa	0.58	0.40	1.03	1.35	0.84	0.84	0.82	0.64	0.83	0.68	0.49	0.49
Muger	0.18	0.17	0.88	1.03	0.80	0.69	0.60	0.44	0.68	0.61	0.61	0.61
Temcha	0.24	0.18	0.44	0.52	0.78	0.78	0.76	0.76	0.67	0.67	0.53	0.53
Kessie	0.62	0.43	0.77	1.01	0.87	0.95	0.87	0.79	0.84	0.74	0.48	0.48
Lower Abay	0.24	0.17	0.42	0.5	0.89	0.8	0.82	0.51	0.80	0.63	0.42	0.70

Table 9. Weighted mean monthly temperature baseline and projected future temperature change for periods 2046–2064 and 2081–2099 in the Blue Nile Basin.

	Baseline	CCCMA 1	CCCMA 2	CRNM 1	CRNM 2	MRI 1	MRI 2
Jan	19.40	23.10	24.30	21.00	22.10	23.10	23.80
Feb	21.00	23.80	24.80	22.50	23.70	23.30	23.70
Mar	22.20	24.00	24.30	23.90	25.20	23.10	23.30
Apr	22.40	23.00	23.40	24.30	25.10	21.90	22.00
May	21.40	21.40	22.10	23.10	23.90	21.00	21.50
Jun	19.50	20.80	22.20	22.10	22.70	20.30	21.10
Jul	17.00	21.40	23.10	21.20	21.90	20.60	21.50
Aug	16.60	21.70	22.50	20.90	21.90	20.70	21.50
Sep	17.40	21.00	21.90	21.00	21.90	20.50	20.50
Oct	17.80	20.80	21.80	21.20	21.90	19.80	20.60
Nov	18.60	20.80	22.00	20.90	21.70	20.00	21.40
Dec	18.60	22.00	23.40	20.60	21.50	21.50	22.90
Mean	19.3	22.0	23.0	21.9	22.8	21.3	22.0
Abs. diff (°C)		2.7	3.7	2.6	3.5	2.0	2.7
Rel. diff (%)		13.72	18.89	13.32	17.97	10.39	13.81

6. Conclusions

Despite improvements in climatic modelling, the findings of this study highlight remaining uncertainty between different GCMs regarding projected changes. The results indicate similar trends, but divergent patterns of precipitation and temperature change. Regarding future temperature changes in the Abay basin, all three GCMS predict increases in mean temperature, including similar temperature peaks and similar drops in mean monthly temperature. Further, all three GCMs project that the main rainy season will gradually decline in intensity, with precipitation becoming more distributed throughout the year. The projected temperature and precipitation changes, in turn, have noticeable impacts on modelled streamflows. Generally, the streamflows are projected to increase, either mildly (+0.71%) or dramatically (+97%). Consequently, baseline streamflows are projected to be higher throughout the year. All in all, this could result in increased water availability for rainfed agriculture, domestic consumption, and hydroelectric production. Sudan and Egypt could also benefit from more constant and increased water flow. Nevertheless, uncertainty remains over how climate change will affect the Blue Nile outflows. This, again, is evidenced by the climate change data applied for analyses in the

https://doi.org/10.1016/j.heliyon.2018.e00771

present study. While the three applied models matched in terms of general trends, they diverged with respect to the outcomes for the basin's monthly precipitation and streamflow. At the same time, despite the large differences in projected (absolute) streamflow values, all the models predict more or less dramatic changes in annual patterns of rainfall and temperature. The results suggest that the policy focus should remain on knowledge generation and adaptation to possible outcomes and on mitigation of climate change impacts.

Declarations

Author contribution statement

Vincent Roth, Tatenda Lemann, Hans Hurni: Conceived and designed the experiments; Performed the experiments; Analyzed and interpreted the data; Contributed reagents, materials, analysis tools or data; Wrote the paper.

Gete Zeleke: Analyzed and interpreted the data; Contributed reagents, materials, analysis tools or data; Wrote the paper.

Alemtsehay Subhatu, Tibebu Kassawmar Nigussie: Contributed reagents, materials, analysis tools or data; Wrote the paper.

Funding statement

This work was supported by the Centre for Development and Environment (CDE) and the Institute of Geography of the University of Bern, Switzerland.

Competing interest statement

The authors declare no conflict of interest.

Additional information

No additional information is available for this paper.

Acknowledgements

We are thankful to the Water and Land Resource Centre (WLRC) in Addis Abeba for providing guidance, support, and data.

References

Abbaspour, K.C., 2005. Calibration of hydrologic models: when is a model calibrated? In: Zerger, A., Argent, R.M. (Eds.), MODSIM05, International Congress on Modelling and Simulation Advances and Applications for Management and Decision Making, pp. 2449–2455.

Abbaspour, K.C., 2015. SWAT-CUP 2012: SWAT Calibration and Uncertainty Programs—A User Manual. Tech. rep. Swiss Federal Institute of Aquatic Science and Technology, Eawag.

Abbaspour, K.C., Johnson, C.A., van Genuchten, M.T., 2004. Estimating uncertain flow and transport parameters using a sequential uncertainty fitting procedure. Vadose Zone J. 3 (4), 1340–1352.

Abbaspour, K.C., van Genuchten, M.T., Schulin, R., Schläppi, E., 1997. A sequential uncertainty domain inverse procedure for estimating subsurface flow and transport parameters. Water Resour. Res. 33 (8), 1879–1892.

Abbaspour, K.C., Vejdani, M., Haghighat, S., Yang, J., 2007. SWAT-CUP calibration and uncertainty programs for SWAT. In: The Fourth International SWAT Conference. Delft, Netherlands, pp. 1596–1602.

Abdo, K.S., Fiseha, B.M., Rientjes, T.H.M., Gieske, A.S.M., Haile, A.T., 2009. Assessment of climate change impacts on the hydrology of Gilgel Abay catchment in Lake Tana basin, Ethiopia. Hydrol. Process. 23, 3661–3669.

Adem, A., Tilahun, S.A., Ayana, E.K., Worqlul, A.W., Assefa, T.T., Dessu, S.B., Melesse, A.M., 2016. Climate change impact on sediment yield in the Upper Gilgel Abay catchment, Blue Nile Basin, Ethiopia. In: Melesse, A.M., Abtew, W. (Eds.), Landscape Dynamics, Soils and Hydrological Processes in Varied Climates. Springer International Publishing, pp. 615–642 (Ch. 28).

Aich, V., Liersch, S., Vetter, T., Huang, S., Tecklenburg, J., Hoffmann, P., Koch, H., Fournet, S., Krysanova, V., Müller, E.N., Hattermann, F.F., 2014. Comparing impacts of climate change on streamflow in four large African river basins. Hydrol. Earth Syst. Sci. 18 (4).

Ali, Y.S.A., 2014. The Impact of Soil Erosion in the Upper Blue Nile on Downstream Reservoir Sedimentation. PhD thesis. Delft University.

Arnold, J.G., Kiniry, J.R., Srinivasan, R., Williams, E.B., Haney, E.B., 2011. SWAT: input/output file documentation.

Arnold, J.G., Moriasi, D.N., Gassman, P.W., Abbaspour, K.C., White, M.J., Srinivasan, R., Santhi, C., Harmel, R.D., Van Griensven, A., Van Liew, M.W.,

 https://doi.org/10.1016/j.heliyon.2018.e00771

Kannan, N., Jha, M.K., 2012. SWAT: model use, calibration and validation. Trans. ASABE 55 (4), 1491–1508.

Arnold, J.G., Srinivasan, R., Muttiah, R.S., Williams, J.R., 1998. Large area hydrologic modeling and assessment. Part 1: model development. J. Am. Water Resour. Assoc. 34 (1), 73–89.

Arsano, Y., Tamrat, I., 2005. Ethiopia and the eastern Nile basin. Aquat. Sci. 67 (1), 15–27.

Azagegn, T., Asrat, A., Ayenew, T., Kebede, S., 2015. Litho-structural control on interbasin groundwater transfer in central Ethiopia. J. Afr. Earth Sci. 101, 383–395.

Bates, B., Kundzewicz, Z., Wu, S., Palutikof, J., 2008. Climate Change and Water. Tech. rep. http://www.citeulike.org/group/14742/article/8861411%5Cn. http://www.ipcc.ch/publications_and_data/publications_and_data_technical_papers.shtml#.UREVW6X7Uy4.

Berehanu, B., Azagegn, T., Ayenew, T., Masetti, M., 2017. Inter-basin groundwater transfer and multiple approach recharge estimation of the upper Awash aquifer system. J. Geosci. Environ. Prot. 05 (03), 76–98.

Betrie, G.D., Mohamed, Y.A., van Griensven, A., Srinivasan, R., Mynett, A., 2011. Sediment management modelling in the Blue Nile Basin using SWAT model. Hydrol. Earth Syst. Sci. 15 (3), 807–818. http://www.hydrol-earth-syst-sci.net/15/807/2011/. http://www.hydrol-earth-syst-sci-discuss.net/7/5497/2010/.

Beyene, T., Lettenmaier, D.P., Kabat, P., 2009. Hydrologic impacts of climate change on the Nile river basin: implications of the 2007 IPCC scenarios. Clim. Change 100 (3–4), 433–461.

Beyene, E.G., Meissner, B., 2010. Spatio-temporal analyses of correlation between NOAA satellite RFE and weather stations' rainfall record in Ethiopia. Int. J. Appl. Earth Obs. Geoinf. 12, 69–75.

Brunner, M., 2012. A National Soil Model of Ethiopia: A Geostatistical Approach to Create a National Soil Map of Ethiopia on the Basis of an SRTM 90 DEM and SOTWIS Soil Data. Master thesis. University of Bern, Switzerland.

Conway, D., 1997. A water balance model of the Upper Blue Nile in Ethiopia. Hydrol. Sci. J. 42 (2), 265–286.

Conway, D., 2000. The climate and hydrology of the Upper Blue Nile river. Geogr. J. 166 (1), 49–62.

Dessie, M., Verhoest, N.E.C., Pauwels, V.R.N., Admasu, T., Poesen, J., Adgo, E., Deckers, J., Nyssen, J., 2014. Analyzing runoff processes through conceptual

hydrological modeling in the Upper Blue Nile Basin, Ethiopia. Hydrol. Earth Syst. Sci. 18 (12), 5149–5167.

Douglas-Mankin, K.R., Srinivasan, R., Arnold, J.G., 2010. Soil and Water Assessment Tool (SWAT) model: current development and applications. Amer. Soc. Agric. Biol. Eng. 53 (5), 1423–1431.

Easton, Z.M., Fuka, D.R., White, E.D., Collick, A.S., Biruk Ashagre, B., McCartney, M., Awulachew, S.B., Ahmed, A.A., Steenhuis, T.S., 2010. A multi basin SWAT model analysis of runoff and sedimentation in the Blue Nile, Ethiopia. Hydrol. Earth Syst. Sci. 14 (10), 1827–1841. http://www.hydrol-earth-syst-sci.net/14/1827/2010/.

Elshamy, M.E., Seierstad, I.A., Sorteberg, A., 2009. Impacts of climate change on Blue Nile flows using bias-corrected GCM scenarios. Hydrol. Earth Syst. Sci. 13 (5), 551–565.

Girvetz, E., Maurer, E., Duffy, P., Ruesch, A., Thrasher, B., Zganjar, C., 2012. Making Climate Data Relevant to Decision Making. Tech. rep. The World Bank. http://sdwebx.worldbank.org/climateportal/doc/Global_Daily_Downscaled_Climate_Data_Guidance_Note.pdf.

Haile, A.T., Rientjes, T.H.M., Gieske, A., Gebremichael, M., 2009. Rainfall variability over mountainous and adjacent lake areas: the case of Lake Tana basin at the source of the Blue Nile river. J. Appl. Meteorol. Climatol. 48 (8), 1696–1717.

Hu, X., McIsaac, G.F., David, M.B., Louwers, C.A.L., 2007. Modeling riverine nitrate export from an East–Central Illinois watershed using SWAT. J. Environ. Qual. 36 (2005), 996–1005.

Hurni, H., 1998. Agroecological Belts of Ethiopia: Explanatory Notes on Three Maps at a Scale of 1:1,000,000. Soil Conservation Research Programme (SCRP). Centre for Development and Environment (CDE), Bern, Switzerland.

Hurni, K., Zeleke, G., Kassie, M., Tegegne, B., Kassawmar, T., Teferi, E., Moges, A., Tadesse, D., Ahmed, M., Degu, Y., Kebebew, Z., Hodel, E., Amdihun, A., Mekuriaw, A., Debele, B., Deichert, G., Hurni, H., 2015. Economics of Land Degradation (ELD) Ethiopia Case Study. Soil Degradation and Sustainable Land Management in the Rainfed Agricultural Areas of Ethiopia: An Assessment of the Economic Implications. Tech. rep. Economics of Land Degradation Initiative.

IPCC (Intergovernmental Panel for Climate Change), 2008. Special Report on Observed and Projected Changes in Climate as They Relate to Water. Tech. rep. Cambridge University Press, Cambridge.

 https://doi.org/10.1016/j.heliyon.2018.e00771

Kassawmar, T., Eckert, S., Hurni, K., Zeleke, G., Hurni, H., 2016. Reducing landscape heterogeneity for improved land use and land cover (LULC) classification across the large and complex Ethiopian highlands. Geocarto Int. 6049, 1–17.

Kebede, S., Travi, Y., Alemayehu, T., Marc, V., 2006. Water balance of Lake Tana and its sensitivity to fluctuations in rainfall, Blue Nile Basin, Ethiopia. J. Hydrol. 316 (1–4), 233–247.

Kim, U., Kaluarachchi, J.J., 2008. Application of parameter estimation and regionalization methodologies to ungauged basins of the Upper Blue Nile river basin, Ethiopia. J. Hydrol. 362 (1–2), 39–56.

Kim, U., Kaluarachchi, J.J., 2009. Climate change impacts on water resources in the Upper Blue Nile river basin, Ethiopia. J. Am. Water Resour. Assoc. 45 (6), 1361–1378.

Krause, P., Boyle, D.P., Bäse, F., 2005. Comparison of different efficiency criteria for hydrological model assessment. Adv. Geosci. 5 (5), 89–97. http://www.adv-geosci.net/5/89/2005/adgeo-5-89-2005.html.

Legesse Gebre, S., Fulco, L., 2015. Hydrological response to climate change of the Upper Blue Nile river basin: based on IPCC fifth assessment report (AR5). J. Climatol. Weather Forecast. 3 (1), 1–15.

Mccartney, M.P., Alemayehu, T., Easton, Z.M., Awulachew, S.B., 2012. Simulating current and future water resources development in the Blue Nile river basin. In: Awulachew, S.B., Smakthin, V., Molden, D., Peden, D. (Eds.), The Nile River Basin. Routledge Taylor and Francis Group, pp. 269–291 (Ch. 14).

Medhin, G., 2011. Livelihood Zones Analysis. Tech. rep. FAO.

Mishra, A., Hata, T., Abdelhadi, A.W., 2004. Models for recession flows in the Upper Blue Nile river. Hydrol. Process. 18 (15), 2773–2786.

Moriasi, D.N., Arnold, J.G., Van Liew, M.W., Bingner, R.L., Harmel, R.D., Veith, T.L., 2007. Model evaluation guidelines for systematic quantification of accuracy in watershed simulations. Trans. ASABE 50 (3), 885–900.

Nawaz, R., Bellerby, T., Sayed, M., Elshamy, M., 2010. Blue Nile runoff sensitivity to climate change. Open Hydrol. J. 4, 137–151.

Neitsch, S., Arnold, J., Kiniry, J., Williams, J., 2011. Soil & Water Assessment Tool Theoretical Documentation Version 2009. Tech. rep. Texas Water Resources Institute, College Station, TX.

Niang, I., Ruppel, O., Abdrabo, M., Essel, A., Lennard, C., Padgham, J., Urquhart, P., 2014. Africa. Tech. rep. IPCC, Cambridge.

Salas-Mélia, D., Chauvin, F., Déqué, M., Douville, H., Gueremy, J., Marquet, P., Planton, S., Royer, J., Tyteca, S., 2005. Description and validation of the CNRM-CM3 global coupled model. Clim. Dyn. 36. http://www.cnrm.meteo.fr/scenario2004/paper_cm3.pdf.

Saleh, A., Arnold, J.G., Gassman, P., Hauck, L.M., Rosenthal, W.D., Williams, J.R., McFarland, A.M.S., 2000. Application of SWAT for the Upper North Bosque river watershed. Trans. ASAE 43 (5), 1077–1087.

Schuol, J., Abbaspour, K.C., Srinivasan, R., Yang, H., 2008. Estimation of freshwater availability in the West African sub-continent using the SWAT hydrologic model. J. Hydrol. 352 (1–2), 30–49. http://linkinghub.elsevier.com/retrieve/pii/S0022169407007755.

Setegn, S.G., Dargahi, B., Srinivasan, R., Melesse, A.M., 2010. Modeling of sediment yield from Anjeni-gauged watershed, Ethiopia using SWAT model. J. Am. Water Resour. Assoc. 46 (3), 514–526.

Siam, M.S., Eltahir, E.A.B., 2017. Climate change enhances interannual variability of the Nile river flow. Nat. Clim. Change 7 (5), 350–354.

Sutcliffe, J.V., Parks, Y.P., 1999. The Hydrology of the Nile. IAHS speci Edition, No. 5. IAHS, Wallingford, Oxfordshire, UK.

Taye, M.T., Ntegeka, V., Ogiramoi, N.P., Willems, P., 2011. Assessment of climate change impact on hydrological extremes in two source regions of the Nile river basin. Hydrol. Earth Syst. Sci. 15 (1), 209–222. http://www.hydrol-earth-syst-sci.net/15/209/2011/.

Taye, M.T., Willems, P., 2012. Temporal variability of hydroclimatic extremes in the Blue Nile Basin. Water Resour. Res. 48 (3), 1–13.

Taye, M.T., Willems, P., Block, P., 2015. Implications of climate change on hydrological extremes in the Blue Nile Basin: a review. J. Hydrol., Reg. Stud. 4, 280–293.

van Griensven, A., Ndomba, P.M., Yalew, S., Kilonzo, F., 2012. Critical review of the application of SWAT in the upper Nile basin countries. Hydrol. Earth Syst. Sci. Discuss. 9 (3), 3761–3788. http://www.hydrol-earth-syst-sci-discuss.net/9/3761/2012/. http://www.hydrol-earth-syst-sci.net/16/3371/2012/.

Van Liew, M.W., Veith, T.L., Bosch, D.D., Arnold, J.G., 2007. Suitability of SWAT for the conservation effects assessment project: comparison on USDA agricultural research service watersheds. J. Hydrol. Eng. 12 (2), 173–189.

Wagena, M.B., Sommerlot, A., Abiy, A.Z., Collick, A.S., Langan, S., Fuka, D.R., Easton, Z.M., 2016. Climate change in the Blue Nile Basin Ethiopia: implications for water resources and sediment transport. Clim. Change 139 (2), 229–243.

 https://doi.org/10.1016/j.heliyon.2018.e00771